Structural evolution of Ni-20Cr alloy during ball milling of elemental powders

I. López-Báez,[a] E. Martínez-Franco,[b] H. Zoz,[c] and L.G. Trápaga-Martínez[a]
[a]*Centro de Investigación y de Estudios Avanzados del Instituto Politécnico Nacional,*
Libramiento Norponiente No. 2000, Fracc. Real de Juriquilla, 76230, Santiago de Querétaro, Qro.,México,
e-mails: israelbaez@gmail.com; trapaga@qro.cinvestav.mx
[b]*Centro de Investigación e Innovación Tecnológica,*
Cerrada de Cecati S/N, Col. Santa Catarina Azcapotzalco, 02250, D.F., México,
e-mail: enmartinezf@ipn.mx
[c]*Zoz GmbH, D-57482 Wenden, Germany*
e-mail: info@zoz.de

Recibido el 6 de diciembre de 2010; aceptado el 28 de febrero de 2011

The ball milling (BM) of blended Ni and Cr elemental powders was carried out in a Simoloyer performing on high-energy scale mode at maximum production to obtain a nanostructured Ni-20Cr alloy. The phase transformations and structural changes occurring during mechanical alloying were investigated by X-ray diffraction (XRD) and optical microscopy (OM). A gradual solid solubility of Cr and the subsequent formation of crystalline metastable solid solutions described in terms of the Avrami-Erofe'ev kinetics model were calculated. The XRD analysis of the structure indicates that cumulative lattice strain contributes to the driving force for solid solution between Ni and Cr during BM. Microstructure evolution has shown, additionally to the lamellar length refinement commonly observed, the folding of lamellae in the final processing stage. OM observations revealed that the lamellar spacing of Ni rich zones reaches a steady value near 500 nm and almost disappears after 30 h of milling.

Keywords: Mechanical alloying; solid solubility; X-ray diffraction; metastability; lamellar refinement.

La molienda por bolas (MB) de la mezcla de polvos elementales Ni y Cr se realizó en un Simoloyer con una configuración de alta energía cinética y máxima capacidad de producción, el propósito fue obtener una aleación nanoestructurada Ni-20Cr. Las transformaciones de fase y los cambios estructurales llevados a cabo durante el aleado mecánico se investigaron utilizando las técnicas de difracción de rayos-X (DRX) y microscopía óptica (MO). Para el comportamiento cinético de la mezcla NiCr, pudo utilizarse el modelo cinético de Avrami-Erofe'ev para ajustar los datos experimentales de la solubilidad sólida del Cr y determinarse de esta manera un estado metaestable al aproximarse a la aleación Ni-20Cr. Los análisis de DRX indican que el almacenamiento de energía mecánica como deformación plástica contribuye con las fuerzas impulsoras para llevarse a cabo la solución sólida Ni(Cr) durante la MB. La evolución microestructural presentó un refinamiento adicional en la longitud de las laminillas concerniente a un doblamiento de las mismas en la etapa final del procesamiento. Las observaciones por MO revelaron que el espaciamiento laminar correspondiente a las zonas ricas en Ni alcanza un valor estable cercano a los 500 nm, y es casi despreciable después de 30 h de molienda.

Descriptores: Aleado mecánico; solubilidad sólida; difracción de rayos-X; metaestabilidad; refinamiento laminar.

PACS: 81.20.Ev; 64.70.K-; 81.30.-t

1. Introduction

Ni-base alloys with coarse grain structure are used for a wide variety of applications, the majority of which involve corrosion, heat, and wear resistance. The number of studies focused on mechanical alloying (MA) by BM of Ni and Cr elemental powders to obtain the Ni-20Cr alloy is scarce, despite the potential applications of this type of alloys. Some experimental studies have shown that the mechanical and electrochemical properties of some Ni-base coatings improved as a result of its nanocrystalline structure. [1,2], particularly oxidation and corrosion for the Ni-20Cr system prepared by MA [3,4].

In MA processes, metals (typically in their elemental form) are mixed by the application of extensive plastic strain, most commonly through ball milling or cold rolling [5]. During milling, the initially crystalline metallic powders agglomerate, proceed to form fine lamellar structures, and with reactive collisions easily induce their atomic-scale mixing. Experimental and theoretical evidences suggest a coupling between mechanical stress, solubility limits and atomic mobility [6,7] to enable the driving forces operating at collisions. The mechanochemical effects, acting during collision, need to be understood to accomplish a satisfactory rationalization of these driving forces, which are connected with the quantification of phase transformation kinetics on both microscopic and macroscopic scales. This issue raises remarkable difficulties, owing to the wide gap separating atomistic studies and phenomenological kinetics investigations in terms of feasibility and accuracy [8]. Badmos and Bhadeshia [9] predicted that solution formation of solid components by MA cannot occur unless there is a gain in coherency as the particles become smaller and eventually disappear as true solution. Schwarz [10] predicted that dislocations induced by plastic deformations act as solute-pumping stations, which introduce solutes into crystalline lattices, even in the presence of a chemical energy barrier.

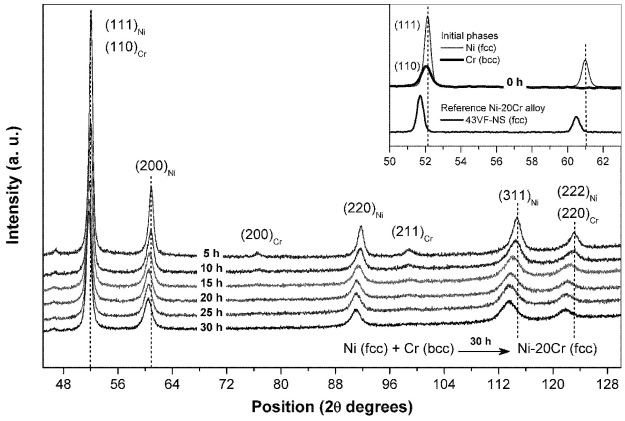

FIGURE 1. XRD patterns of Ni-Cr at different milling times and commercial reference.

Different experimental techniques have been used to understand phase transformations during MA. Vasconcelos and de Figueiredo [11] have shown that the volume fraction of two binary systems has a gradual dissolution; they also identified several stages deduced by magnetic hyperfine field distributions obtained by Mössbauer spectroscopy. On the other hand, Delogu [12] observed a gradual dissolution with a subsequent formation of crystalline metastable solid solutions using XRD patterns fitted with the Rietveld method. The two techniques mentioned above are commonly used to obtain the evolution of structural parameters linked to the dissolution process for elucidating the mechanisms of alloy formation.

Understanding the phase formation kinetics and processes is still complicated, because numerous parameters govern the MA process. The Johnson Mehl Avrami model has been commonly used to describe the kinetics of the volume fraction transformed [13]. The studies on this matter are supported by experimental results, although there is scarce evidence about the influence of controlled milling parameters on powder microstructure using large mill capacities [14,15], despite the benefits that this would bring to large scale production. In most cases, the experimental phase transformation kinetics and microstructure evolution studies are based on particular semi-controlled milling parameters (temperature) and small mill capacities [8,12,13].

Accordingly, the purpose of this work was to study the phase transformation, crystal structure and microstructure changes taking place during the MA of elemental Ni and Cr powders to achieve a Ni-20Cr alloy in a Simoloyer performing on high-energy scale mode at maximum production. The optimal production conditions used can be scaled up in a higher capacity Simoloyer to obtain large quantities of this alloy thereby increasing their potential application. In this study, XRD analysis was used to follow structural changes associated with the formation of solid solution from the crystallite size and lattice strain evolution. Also, an attempt to study the mechanism and kinetics of Cr dissolution into the Ni matrix was carried out through the determination of the Avrami-Erofe'ev parameter, n. In addition, OM was used to ascertain the distribution of new phases produced during BM.

2. Experimental procedures

BM of elemental Ni powder (ALFA AESAR, particle size less than 37 μm with 99.8% purity) and Cr powder (ALFA AESAR, particle size less than 44 μm with 99% purity) in the required weight ratio (4:1) was conducted using a horizontal attritor commercially known as Simoloyer CM01 (Zoz GmbH, Wenden, Germany) and 600 g of bearing steel balls with 4.7 mm diameter. The high ductility of Ni makes difficult the BM under argon atmosphere because the material adheres onto the stainless steel vessel wall (0.5 l of volume capacity). The use of operating cycles abated this event, by changing the milling velocity periodically to improve the milling efficiency and thus enabling the maximum loading of 100 g of a manual mixture of elemental powders. An operation cycle in this study is characterized by a time interval of 3 min at 1800 rpm followed by 1 min of operation at 1000 rpm. The Simoloyer cooling system used water at room temperature.

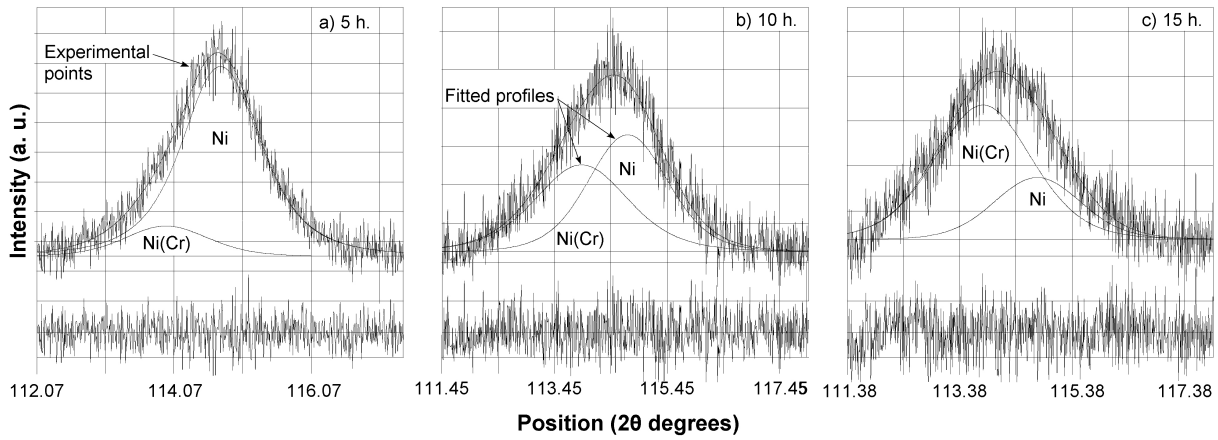

FIGURE 2. Details of the observed fcc (311) reflection peak profiles at different milling times.

TABLE I. Diffraction peak positions of the analyzed powders.

Powder	Position (2θ degrees)				
	(111)	(200)	(220)	(311)	(222)
Initial fcc Ni	52.08	60.94	91.72	114.64	123.11
Final fcc Ni-20Cr	51.71	60.40	90.95	113.40	121.50
43VF-NS as reference	51.68	60.44	90.90	113.38	121.59

Morphological and chemical analyses were performed with a Philips/XL30ESEM microscope (high vacuum, 30 kV), and with the energy dispersive spectroscopy of X-rays (EDS), respectively. The structural analysis in samples at different processing times was done using a Rigaku/Dmax2100 diffractometer with Co-Kα_1 radiation, and a scanning transmission electron microscopy (TEM) analysis was carried out to reveal the nature of sub-grain (crystallite) size of the final alloy in a Philips/CM-200, operated at 200 kV. Differential scanning calorimetry (DSC) analysis was done in a Mettler Toledo (DSC822e) calorimeter. Samples at different milling times were mounted in resin, prepared metallographically and etched with HF/HNO_3 (1/4 in volume) to show their microstructure using OM. A commercial powder alloy (Metco 43VF-NS Ni-20Cr, manufactured by water atomization) was used as reference. The Buehler MMT-3 digital microindentation hardness tester was used to measure microhardness.

3. Results and discussion

3.1. Crystal structure

Figure 1 shows XRD patterns of unmilled elemental powder (0 h) and their evolution as a result of solid solution formation during BM to obtain an approached Ni-20Cr alloy. After 5 h of milling, both characteristic peaks of fcc Ni and bcc Cr are observed, indicating that at this milling time only refinement occurs. As the milling process progresses, the initially sharp diffraction peaks are broadened and reduced in intensity because of the spatial coherent length confinement and the increase in atomic level strain. Both features originated from the repeated fracturing and cold welding of particles, are explained by their severe plastic deformation. In addition, the diffraction peaks of the fcc Ni phase shift to the smaller angles for milling times larger than 5 h according to the reference alloy; this points out to an increase of the Ni lattice parameter attributable to the structural distortions induced by the progressive diffusion of Cr into the fcc Ni matrix leading to the formation of the Ni(Cr) solid solution. Furthermore, the Bragg diffraction peaks of the bcc Cr are broadened, reduced in intensity and still visible until 25 h of milling. This result suggests that the alloy formation occurs in a solid state during milling. Table I presents a comparison of angular position of initial (Ni), final (Ni-20Cr at 30 h), and reference (commercial alloy 43VF-NS) fcc phases, where the angular positions of the initial fcc phase (Ni) decrease by atomic substitution induced by MA (Cr solubility) until approaching the reference peak positions.

XRD patterns of unmilled powders indicate an overlapping of the $(111)_{Ni}$ and $(110)_{Cr}$ reflection peaks with a little shift on angular positions after their milling. On the other hand, broadened and asymmetric peak displacements are markedly observed on high angles. It has been shown, that phase volume evolution analyses on high angles using deconvolution of diffraction profiles is a reliable technique to quantify the evolution of solid solution formation [16]. This technique has been applied to quantify the evolution of fcc Ni(Cr) and fcc Ni phases in the experimental samples because does not required complicated software calculations and/or knowledge of specific structural parameters. Hence, it is practical to determine the alloy state in the horizontal mill. The procedure consists in modeling the diffraction profiles by an analytical function to characterize the microstructure of the powders. The asymmetric peaks can be fitted using the Pearson VII distribution function (WinFit 1.2.1. program) with kα_2 correction and 95% reliability as minimum. The fitting procedure is based on the next considerations during milling: i) fcc Ni peak intensity decreases, ii) amorphous forming range increases, iii) angular position of milled fcc Ni phase contribution is nearest to the unmilled fcc Ni phase ($2\theta \approx 114.637$ degrees), iv) angular position of the Ni(Cr) phase shifts to the smaller angles, and v) both fitted profiles are similar in shape. In light of these considerations, the deconvolution of asymmetric diffraction profiles and the analysis of the peaks related to each phase are relatively easy to apply for monitoring the material processing.

The fitting procedure results are shown in Fig. 2 for the fcc (311) reflection for different milling times; where the changes in the relative contributions of Ni and Ni(Cr) phases are clearly defined. Initially, the XRD peak profile becomes asymmetric on its low-angle shoulder, which may be explained by the appearance of a broad and low intensive peak on the left side of the Ni peak. This additional peak can be attributed to a new phase that possesses the same structure type as the Ni but is characterized by a slightly larger lattice parameter. Thus, the new phase is the fcc Ni(Cr) solid solution. The Ni(Cr) peak is very broad, typical of a crystal heavily deformed by the solid solution process [17].

After 25 h of the MA process, the Cr (211) peak completely disappears (Fig. 1); the remaining profiles are negligible asymmetric and related to the final Ni(Cr) phase and the Ni phase trace according to profile evolution. The Ni(Cr) (222) reflection peak was also analyzed; however, the Ni and Cr diffraction peaks are overlapped in this angular position. Therefore, to fit and analyze the milled samples, for which intensity of Cr peak is little lower that Cr (220) but still significant (Fig. 1), the Ni (222) reflection peak profile is taken into account, but only expecting a negligible effect of texture on the relative intensity of diffraction profiles for the milled powders.

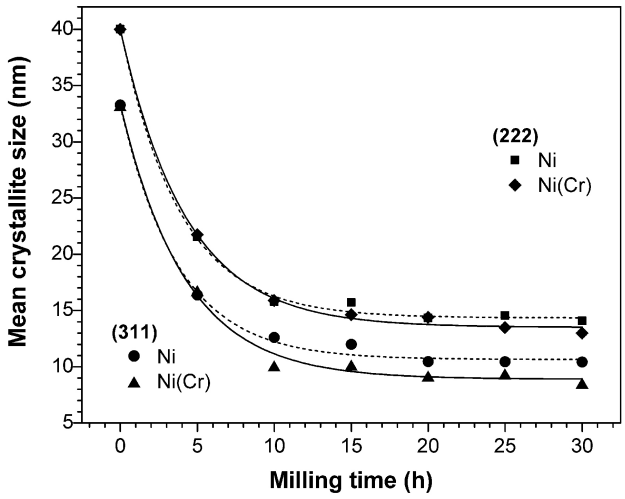

FIGURE 3. Mean crystallite size of Ni and Ni(Cr) phases on (311) and (222) reflections.

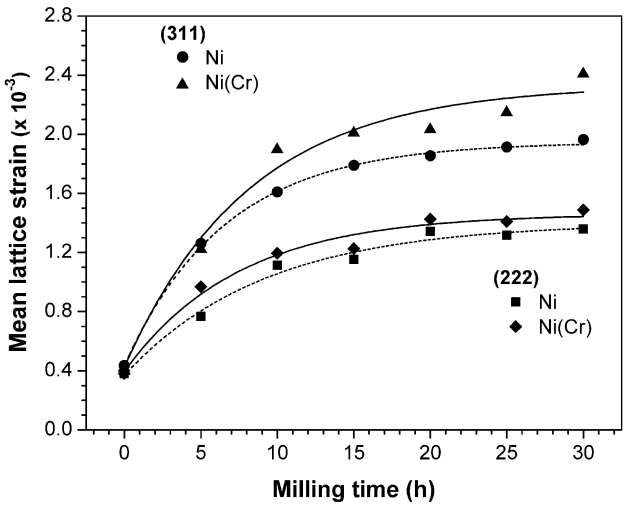

FIGURE 4. Mean lattice strain of Ni and Ni(Cr) phases for the (311) and (222) reflections.

Mean crystallite size and lattice strain from XRD fitted profiles are obtained from:

$$D_v = \frac{\lambda}{\beta^C \cos\theta} \tag{1}$$

$$e = \frac{1}{4}\beta^G \cot\theta \tag{2}$$

Where, $D_v$is the volume-weighted average crystallite size, λ is the wavelength, e is the weighted average strain value, β^C is the integral breadth of the size broadened profile (Cauchy component), and the β^G is the integral breadth of the strain broadened profile (Gaussian component), which are calculated by an approach of Keijser *et al.* [18].

The cumulative deformation energy is supplied by the BM causing changes in metal crystallite size and lattice strain. Figure 3 shows the mean crystallite size of Ni and Ni(Cr) phases in different crystal planes versus milling time. The crystallite size decreases rapidly during the first 10 h of milling process to an approximate value of 16 nm for (222) and 10–13 nm for (311) reflections, then drops slightly up to 20 h of milling and afterwards remains milling-time independent. Figure 4 shows the mean lattice strain versus milling time of the Ni and Ni(Cr) phases in different crystal planes. The lattice strain increases gradually during the first 15 h of milling and then reaches some asymptotic value. Moreover, during milling the Ni lattice strain is lower than that of the Ni(Cr), and the Ni crystallite size (Fig. 3) is higher than that of the Ni(Cr).

All these events can be accounted for by the mechanism of crystallite size reduction at high strain rates process, in which the structural refinement is strongly inhomogeneous and might occur in shear bands of high dislocation density surrounded by less-deformed regions [17]. An increase of dislocation density with an average dislocation distance of a few nanometers is present in the shear bands (initial milling times). This distance is within the range of the final crystallite size after long milling times. The shear bands grow with long milling times; eventually a rearrangement of dislocations creates grain boundaries and the absorption of dislocations as secondary grain boundary dislocations (sub-grain) [17]. Therefore according to this mechanism, the earliest shear bands (high dislocation density) induce measured crystallite size (Fig. 3) that decreases rapidly while the cumulative lattice strain (Fig. 4) gradually achieves a saturation level. Furthermore, most cumulative lattice strain (lower crystallite size) takes place in the Ni(Cr) phase because of the introduction of the Cr atoms by diffusion in the Ni phase.

The kinetics of Cr dissolution into the Ni matrix and the consequent formation of the Ni(Cr) solid solution can be deduced from the XRD fitted profiles. Figure 5 shows the transformation of the Ni(Cr) phase versus milling time. Some known steps of the solid state reaction kinetics are partially identified: i) the induction period, usually regarded as being terminated by the development of stable nuclei and negligible for this case (often completed at a low value of fractional decomposition); ii) the acceleratory period of growth of such nuclei, perhaps accompanied by further nucleation, and which extends to the maximum solubility rate of reaction; iii) the decay period, where the continued expansion of nuclei is no longer possible, owing to impingement and consumption of reactant that leads to deceleration; iv) the deceleratory period, which continues until completion of reaction. The maximum dissolution rate of Cr atoms into the Ni matrix was obtained from the derivative of the Ni(Cr) fitted curve. As can be seen in Fig. 5, Ni(Cr) fraction increases with milling time, revealing the progressive dissolution of the Cr into the Ni matrix as milling proceeds. Regarding the rate of Cr dissolution, it increases with milling and reaches a maximum value between 8–9 h. This can be explained by the significant reduction of crystallite size and the introduction of an important amount of lattice defects at this stage, which enhances the Cr atoms diffusion into the Ni matrix. Afterwards, the Cr dissolution rate decreases with milling time due to the consumption of the Cr atoms, tending to a complete diffusion and therefore to the formation of the final Ni(Cr) phase.

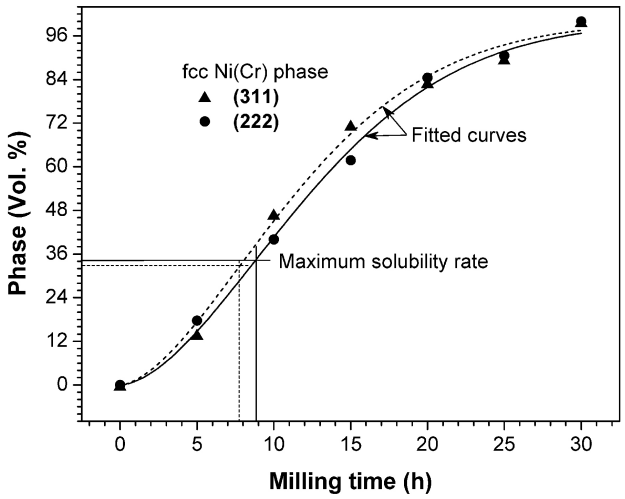

FIGURE 5. Evolution of Ni(Cr) fraction versus milling time.

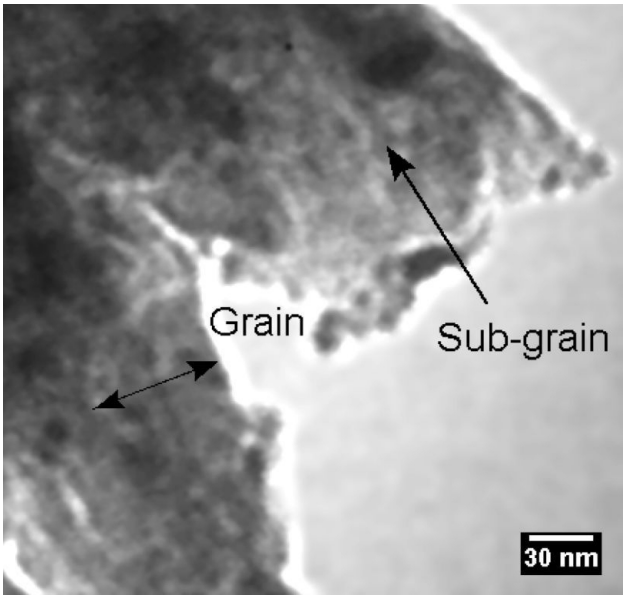

FIGURE 6. TEM bright-field images of the Ni(Cr) at 30 h of milling.

According to our results, the solid solution formed approaches asymptotically to 100% at about 30 h of milling process. Results shown in Fig. 5 suggest that after this processing time there will not be any easily discernible changes in the amount of transformed phase revealed by XRD analysis. A metastable structure is then expected because the Ni(Cr) steady state begins. Hence for practical purposes the milling time needed to produce the solid solution by BM under performed experimental conditions is 30 h.

The behavior of the Cr transformed fraction with milling time can be fitted with the Avrami-Erofe'ev (AE) rate equation commonly used in kinetics analysis of isothermal reactions of solids. The parameters of this equation allow us to determine the relation between nanoscale formation mechanisms and severe plastic deformation induced by the Simoloyer configuration. The transformed fraction exhibits a time dependence of the form:

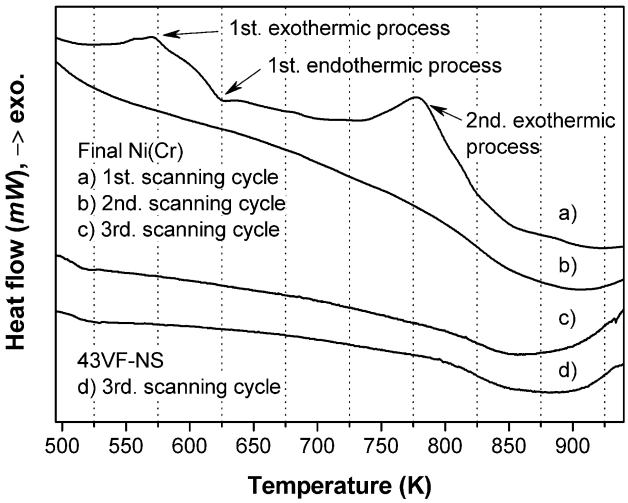

FIGURE 7. DSC analysis of the Ni(Cr) at 30 h of milling and 43VF-NS as reference.

$$f = 1 - e^{-[k(t-t_0)]^n} \tag{3}$$

Where, f is the volume fraction transformed, t the milling time, t_0 is the induction time for the reaction, k the rate constant, and the exponent n is the order of the reaction with $n = \beta + \gamma$, where β is the number of steps involved in nucleus formation and γ is the number of dimensions in which the nuclei grow. These parameters were obtained using the Sigmoidal-Weibull function from fitting procedure. The Avrami fit of the Cr transformed fraction is obtained with the following kinetics parameters: n = 1.71 and k = 0.068 for the (222) reflection; n = 1.66 and k = 0.073 for the (311) reflection. According to Hulbert [19], for n ranging from 1 to 2, lath-shaped particles (γ= 1) of reactant with a decelerator nucleation rate is the model for controlled growth process by nucleation and diffusion. In the case of BM, the lath-shaped particles of reactant could be similar to the shear bands induced by severe plastic deformation related to the mechanism of crystallite size reduction at high strain rates process. According to the BM, β tends to 0 because the solid state reaction occurs rapidly whenever the powder particles are trapped between milling tools to form the solid solution. However, the operating cycles changes the milling intensity; hence the diffusion at low intensity takes place in the new interfaces formed by the high intensity. Thus, it appears that the prevailing reaction mechanisms are the interface diffusion and the diffusion through dislocations and grain boundaries (crystallite size reduction).

Figure 6 presents a bright-field scanning TEM micrograph of the final Ni(Cr) alloy at 30 h of milling, with a microstructure consisting of an homogeneous distribution of nanoscale particles with sub-grain sizes ranging from 10 to 15 nm, corroborating the mean crystallite size calculated by Eq. (1).

In order to allow thermal stability and oxidation behavior comparison of commercial powders and the experimental alloy after 30 h of milling, three thermal cycles for both

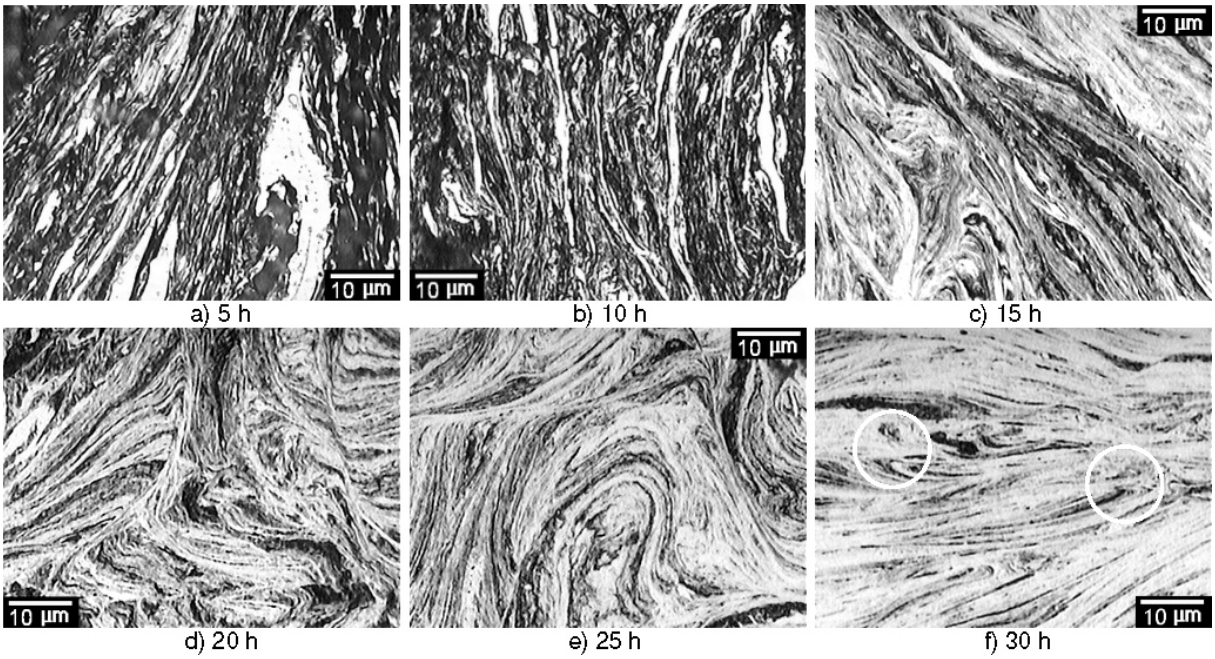

FIGURE 8. Optical images of cross section of powder particles with etching.

powders were carried out: two heating cycles in argon atmosphere to release the stored deformation energy, as will be mentioned below, and a final heating cycle in oxygen atmosphere to explore the oxidation resistance.

Figure 7 shows DSC scans performed at a heating rate of 10 K/min and different atmospheric conditions for milled Ni-20Cr and the reference samples. Several thermal processes were observed for the milled Ni-20Cr in the first temperature scanning cycle in argon. According to Lang *et al.* [20], the first exothermic process (broad peak) is related to the short-range ordering, apparently as a result of displacements of Cr atoms due to the interaction with quench vacancies present in high concentrations. According to Klement *et al.* [21], it is attributed to the formation of nuclei for subsequent growth by grain boundary relaxation and sub-grain coalescence. The next thermal process is an endothermic peak, linked to the Curie temperature of Ni traces observed at 627 K. The second exothermic peak, according to Lang *et al.* [20], is related to an additional ordering caused by the self-diffusion of Cr atoms. A further increase in temperature augments the diffusion rate to such an extent that the process of disordering begins and is manifested as a shallow and very broad endothermic peak at intermediate temperatures [20] like the observed one of 873 K. Therefore, DSC curves show the beginning of structural relaxation processes at about 500 K and at 700 K of the milled Ni-20Cr.

Finally, the thermal stability of both alloys is observed in the third temperature scanning cycle in oxygen with much reduced or non-existent ferromagnetism and an exothermic peak, related to oxidation processes, which begins to appear at about 850–950 K [23]. A similar thermal and oxidation behavior can be noted with respect to the reference alloy (43VF-NS), showing that the experimental alloy has reached the expected properties after 30 h of milling. The DSC results thus support the existence of a metastable structure in the experimental sample, as was predicted by XRD analysis.

Complementary characterization was performed by EDS microanalysis. Milling contamination occurred mainly by Fe and Cr, and the Ni/Cr ratio being approximately 3.84 due to Cr contamination from the wear of the milling tools during the material processing. However, according to our DSC results, the thermal and chemical effects due to the process contamination into experimental material are negligible after the thermal cycles.

3.2. Microstructure

The mechanism of alloy evolution strongly depends on the morphology and manufacture of the initial powders [5]. MA of metals is known to be a lamellar process, in which the lamellar spacing decreases during milling; however, if the initial powders have a small particle size and a narrow size distribution, the lamellar spacing evolution will be enabled by an increased contact surface between powder particles, hence the processing time decreases. These conditions can be seen on below microstructural results.

The shape, size, and constituent distributions of the NiCr mixture evolve with milling time, as shown in Fig. 8, where the etching cross sections of powders are presented. Superficial corrosion on samples is visible as dark zones (oxidation by etchant) corresponding mainly to Ni traces. Some comments can be summarized from the microstructure refinement observations, which the refinement consist in decreasing lamellas length and spacing by means of severe plastic

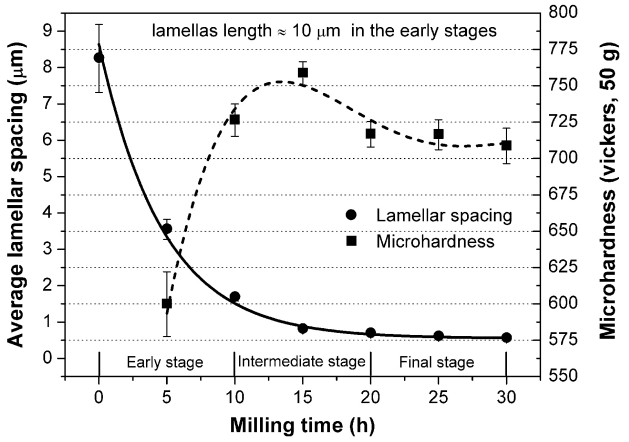

FIGURE 9. Microhardness and average lamellar spacing progress.

deformation induced by the BM. Sample observations of microstructural evolution include: i) soft metal powder particles are welded and flattened by the impacted balls, forming a lamellar structure constituted by small and large particles at 5 h of milling. Furthermore, the chemical behavior of composite particles varies considerably from particle to particle and inside them; ii) lamellas are formed by small and long particles at 10 h of milling; iii) with continued milling, the cold welding and fracturing events continue to take place, leading to microstructural refinement. At this stage, the powder particles consist of convoluted lamellae, as shown in Fig. 8c, and finally, iv) the lamellae become finer and more convoluted, showing possible resistance to the etchant due to Cr solubility increase, which appears as light zones that become larger during milling (Figs. 8d to 8f).

There are also little zones with curved lamellas (represented as white circles drawn in the Fig. 8f), short lamellas length, and dark microzones (random and metastable solid solution). These zones suggest that the lamellas length of powders milled at 30 h is segmented not only by fracturing but also by folding; the lamellas are curved by mechanical deformation until sharp angles are achieved. The chemical heterogeneity in the structure (represented as a dark phase) in these powders indicates the presence of zones with low strain rate, while chemical homogeneity in light zones with high corrosion resistance is linked to the experimental Ni-20Cr alloy with a sub-grain size between 10–15 nm calculated from XRD pattern, and according to Rao *et al.* [23], a lamellar spacing in a nanoscale order is achieved. One would expect the lamellar spacing to become nanometric when the milled powder particles finally become extremely fine and acquire a flaky shape.

The behavior in the lamellar spacing average of Ni rich zones (dark zones in Fig. 8) versus the milling time is shown in Fig. 9. The lamellar spacing in the milled powder particles continuously decreased from an initial value of 8.5 μm of unmilled powders to 500 nm after 30 h of milling. In the early processing stage, the lamellar spacing is rapidly reduced owing to a low cumulative plastic strain; in the intermediate stage, a strain saturation level is achieved and in the final stage, a lamellar spacing of Ni rich zones is only measured because individual lamellae of Ni(Cr) cannot be resolved by OM owing to their extreme thinning of lamellae during the material processing [23]. Therefore, the original Ni and Cr particles or their solid solutions in the course of milling stages are expected to have a nanoscale substructure within their lamellae through which an enhanced diffusion mechanism can occur. The enhanced diffusion is due to: i) nanoscale distances between individual lamellas and their crystallites over which the atoms diffuse, ii) a high diffusivity in the milled material that results from the very high cumulative plastic strain and its associated crystallite size, and iii) the probable temperature rise in milling powders.

When cumulative plastic strain reaches a critical level, the possibility of dynamic recrystallization, which takes place in the synthesis of nanocrystalline sub-grain sizes in metals [5], is expected, and in this particular case a transcendent change in microhardness can occur due to controlled milling temperature by the cooling system. Microhardness (Fig. 9) increases rapidly in the early processing stage as a consequence of the initial cumulative plastic strain linked to lamellar spacing reduction. On the other hand, when lattice strain and lamellar spacing reach a critical level at 15 h, the microhardness achieves a maximum value with a very small change in crystallite size (Fig. 3) and lattice strain (Fig. 4). Thus, results suggest a negligible dynamic recrystallization that takes place after 15 h until microhardness drops and attains a stable value.

4. Conclusions

From a practical standpoint, the study of high diffraction angles peaks provides an alternative to monitoring the chromium solubility in nickel through the evolution of an initial fcc phase and determining the alloy state. Experimental results support the production of a nanostructured Ni-20Cr alloy using a Simoloyer performing on high-energy scale mode at maximum production with a potential as raw material. The main conclusions from the results of material processing are:

- The processing time to produce a nanostructured Ni-20Cr alloy by BM is 30 h. The experimental alloy exhibited thermal and oxidation behaviors similar to those of the reference alloy according to DSC results.

- DSC results also support the existence of a metastable structure in the alloy produced at 30 h of milling, as was predicted by XRD analysis and showed by OM as a chemical heterogeneity with a lamellar spacing of 500 nm.

- Solid state reaction kinetics indicates that the prevailing reaction mechanisms are the interface diffusion and the diffusion through dislocations and sub-grain boundaries (crystallite size reduction was corroborated by TEM micrograph of final milled alloy).

- The BM induced a lamellar structure through all material processing. Some lamellas are curved by mechanical deformation until sharp angles are achieved, indicating the lamella folding as an additional refinement mechanism.
- Microhardness evolution of material indicates that a negligible dynamic recrystallization occurs after 15 h. Then, as the milling process progresses a stable value is reached.

Acknowledgments

The authors acknowledge the technical assistance of A. Galindo-Sifuentes, A. Muñoz-Salas, and Cotroma S.A. de C.V. This work has been supported by Conacyt-Mexico (Projects No. 45246 and 182738).

1. L. Liu, Y. Li, and F. Wang, *Elect. Acta* **52** (2007) 2392.
2. H. Li and F. Ebrahimi, *Acta Mater.* **54** (2006) 2877.
3. G. Fu, Q. Liu, Y. Su, and L. Cai, *Rare Met. Mater. Eng.* **38** (2009) 1150.
4. G.Y. Fu, Q. Liu, B.J. Men, and L. Cai, *Corros. Sci. Prot. Tech.* **18** (2006) 396.
5. C. Suryanarayana, *Mechanical alloying and milling* (Marcel Dekker, New York, United States of America, 2004).
6. M.F. Horstemeyer, M.I. Baskes, and S.J. Plimpton, *Acta Mater.* **49** (2001) 4363.
7. S. Odunuga, Y. Li, P. Krasnochtchekov, P. Bellon, and R.S. Averback. *Phys. Rev. Lett.* **95** (2005) 045901.
8. F. Delogu, *Acta Mater.* **56** (2008) 905.
9. A.Y. Badmos and H.K.D.H. Bhadeshia, *Metall. Mater. Trans. A* **28** (1997) 2189.
10. R.B. Schwarz, *Mater. Sci. Forum* **269-272** (1998) 665.
11. I.F. Vasconcelos and R.S. de Figueiredo, *J. Phys. Chem. B* **107** (2003) 3761.
12. F. Delogu, *Acta Mater* **56** (2008) 2344.
13. H. Moumeni, S. Alleg, and J.M. Grenéche, *J. Alloys Comp.* **419** (2006) 140.
14. K. Maweja, M. Phasha, and N. van der Berg, *Powder Tech.* **199** (2010) 256.
15. S. Hung-Hua, H. Le-Chun, and S. Jiun-Rung, *J. Alloys Comp.* **469** (2009) 483.
16. M. Krasnowski, A. Grabias, and T. Kulik, *J. Alloys Comp.* **424** (2006) 119.
17. C.C. Koch, *Nanostructured materials processing, properties, and applications* (William Andrew Publishing, Nueva York, United Stated of America, 2007).
18. TH.H. de Keijser, E.J. Mittemeijer, and H.C.F. Rozendaal, *J. Appl. Cryst.* **16** (1983) 309.
19. S.F. Hulbert, *J. Brit. Ceram. Soc.* **6** (1969) 11.
20. E. Lang, V. Lupinc, and A. Marucco, *Mater. Sci. Eng. A* **114** (1989) 147.
21. U. Klement, U. Erb, A.M. El-Sherik, and K.T. Aust, *Mater. Sci. Eng. A* **203** (1995) 177.
22. G. Calvarin, R. Molins, and A.M. Huntz, *Oxid. Metals* **53** (2000) 25.
23. M.A. Rao, S. Bhargava and D. Deva, *Metall. Mater. Trans. A* **36** (2005) 3195.